Inorganic Chemistry Communications 179 (2025) 114779

Contents lists available at ScienceDirect

Inorganic Chemistry Communications

journal homepage: www.elsevier.com/locate/inoche

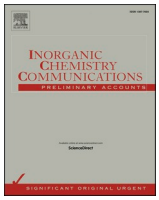

Research Article

Machine learning-guided photocatalytic degradation of Eriochrome Black T using green Nb_2O_5-NPs@CeO_2-NPs

Adriano Losekann Mota Nunes [a], Leandro Rodrigues Oviedo [a], Maurício Dalla Costa Rodrigues da Silva [a,b], Cristiane dos Santos [a], Giovani Pavoski [c], Denise Crocce Romano Espinosa [c], William Leonardo da Silva [a,*]

[a] Applied Nanomaterials Research Group (GPNAp), Franciscan University (UFN), Santa Maria, RS, Brazil
[b] Federal University of Health Sciences of Porto Alegre (UFCSPA), Porto Alegre, RS, Brazil
[c] Polytechnical School of Chemical Engineering, University of the Sao Paulo, São Paulo, SP, Brazil

ARTICLE INFO

Keywords:
Nanotechnology
Advanced oxidation processes
Machine learning
Extreme gradient boosting

ABSTRACT

This study aims to synthesize a green niobium-based catalyst doped with cerium oxide nanoparticles (Nb_2O_5-NPs@CeO_2-NPs) for Eriochrome Black T (EBT) dye degradation under visible radiation and to propose a degradation reaction pathway by machine learning. Nb_2O_5-NPs@CeO_2-NPs were characterized by X-Ray diffraction analysis (XRD), zero-charge point (pH_{ZCP}), Field Emission Gun Scanning Electron Microscopy (FEG-SEM) coupled with Energy Dispersive Spectroscopy (EDS), Diffuse reflectance spectroscopy (DRS), N_2 porosimetry and zeta potential (ZP). The algorithms Decision tree (DT), Random Forest (RF), and Extreme Gradient Boosting (XGBoost) were used to identify the main degradation products of EBT degradation. The incorporation of CeO_2-NPs onto the Nb_2O_5-NPs reduced the band gap from 2.89 to 2.44 eV, resulting in a stable nanocatalyst (ZP = −22.7 mV). Similarly, S_{BET} increased from 19 to 102 $m^2\ g^{-1}$, and D_p from 8.5 to 9.25 nm. However, V_p reduced from 0.04 to 0.2 $cm^3\ g^{-1}$. Nb_2O_5-NPs@CeO_2-NPs showed pH_{ZCP} 6.54, which justifies the higher EBT degradation in the photocatalytic assay (pH 5), probably due to higher electrostatic interactions. Moreover, 68 % EBT degradation (k = 0.0101 min^{-1}) was achieved after 120 min, with good photocatalytic activity up to 3 cycles. $O_2^{\bullet-}$ and h^+ showed a key role in the EBT degradation reaction. RF algorithm showed the best performance among the ML algorithms ($R^2_{training}$ = 0.9539 and R^2_{test} = 0.8364) and lower RMSE ($RMSE_{training}$ = 25.46 and $RMSE_{test}$ = 49.24). Therefore, the nanocatalyst is promising catalytic activity and machine learning is a useful tool for photocatalytic applications.

1. Introduction

Wastewater contaminated with dyes used in industries, mainly textile and chemical, poses a risk to the environment, generating several negative impacts on living beings and their aquatic habitats [1]. Synthetic organic dyes, such as Eriochrome Black T (EBT) are toxic agents for beings in water bodies, as they cause questionable and serious eye problems, promote the imbalance of aquatic ecosystems and photosynthetic process [2]. EBT is an anionic dye and, like other dyes, is chemically stable and has low biodegradability, and is therefore difficult to remove by conventional wastewater treatments due to its great chemical stability [3].

In this context, advanced processes (AOPs) emerge as an alternative for water treatment, such as heterogeneous photocatalysis, widely researched and used for the degradation of dyes in aqueous media, through the generation of free oxygen radicals (hydroxyls, $HO^{\bullet}$, and superoxide radicals, $O_2^{\bullet-}$) with high reducing power, on the surface of a semiconductor (catalyst), when photoactivated under ultraviolet or visible radiation [4].

In parallel, the use of nanomaterials in heterogeneous photocatalysis has considerably improved the efficiency of the process, due to the combination of their properties favorable to heterogeneous photocatalysis, such as low band gap energy (1.5–2 *eV*) and high surface area (50–100 $m^2\ g^{-1}$), mainly due to the combination of ceramic matrices with metal oxide reinforcements [5].

Niobium(V) oxide nanoparticles (Nb_2O_5-NPs) are one of the widely used nanocatalysts in the photodegradation of dyes, mainly due to their physicochemical and thermal stability, acidity and optical activity. In

* Corresponding author.
E-mail address: williamleonardo_silva@hotmail.com (W.L. da Silva).

https://doi.org/10.1016/j.inoche.2025.114779
Received 14 March 2025; Received in revised form 14 May 2025; Accepted 28 May 2025
Available online 29 May 2025

Table 1
Technical details of the ML algorithms.

Algorithm	Algorithm parameters	Equations	Reference
Decision Tree (DT)	Tree maximum depth*: 3, 5, 10, 12, 15 m Number of splits per tree: 2, 3, 5, 7, 10 Performance measured by minimizing the mean squared error R(T), according to Eq. (4)	$R(T) = \frac{1}{N}\sum_{t\in T}\sum_{t\in T}(y_i - \hat{y}_i)^2$ (4)Where: *R(T)* = Expected value of the sum of mean squared errors using a constant as a predictive model; *N* is the number of nodes used in the decision/pattern recognition in the data (one node is equivalent to one leaf of the decision tree); y_i = observed value obtained experimentally; $\hat{y}_i$ = predicted value obtained from the model; t = identifier of each node, T = mean squared error between the observed and the predicted values (response).	[19]
Random Forest (RF)	Tree maximum depth: *: 3, 5, 10, 12, 15, m Number of decision trees tested: 25, 50, 75, 100 Performance measured by minimizing the mean squared error R*(T)*, according to Eq. (5–7)	$R_i(T) = \frac{1}{N}\sum_{t\in T}\sum_{t\in T}\left(y_{pred,i} - y_{obs,i}\right)^2$ (5)$R_j(T) = \frac{1}{N}\sum_{t\in T}\sum_{t\in T}\left(y_{pred,j} - y_{obs,j}\right)^2$ (6)$R_{avg}(T) = \frac{R_i(T) + R_j(T)}{2}$ (7)Where: $R_i(T)$ and $R_j(T)$ are the measurements of the performance of groups *i* and *j* of k-decision trees; $R_{avg}(T)$ is the final response of the RF algorithm (average of the decisions of the n–groups made up of k–trees)	
Extreme Gradient Boosting (XGBoost)	Tree maximum depth: 1, 2, 3, 4, 5 Number of decision trees tested: 25, 50, 75, 100 Learning rate: 1%, 2%, and 3% Method used to prevent overfitting: L2 regularization with λ = 0.2* Subsamples: 80% of the dataset Performance measured by minimizing the mean squared error R*(T)*, as defined in RF algorithm	This algorithm uses several decision trees, divided in k-groups of n–elements, generating a particular answer (decision i, j, k). The algorithms use optimization functions that guarantee greater computational power, fast convergence to the optimal value predicted by the algorithm and less probability of overfitting Response = average of the decisions of the n–groups made up of k-trees	

Random state = 42 for all algorithms tested | * This value represents 20% of the relative weight assigned to the penalization, aiming to balance model complexity.

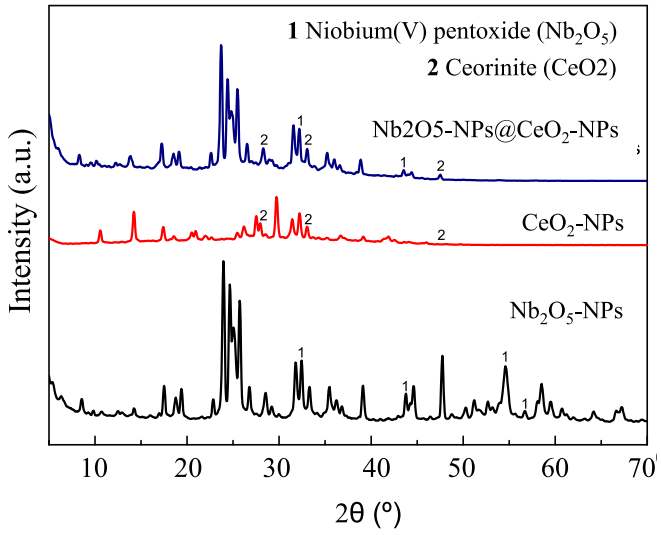

Fig. 1. XRD diffractograms of the Nb_2O_5-NPs, CeO_2-NPs, and Nb_2O_5-NPs@CeO_2-NPs.

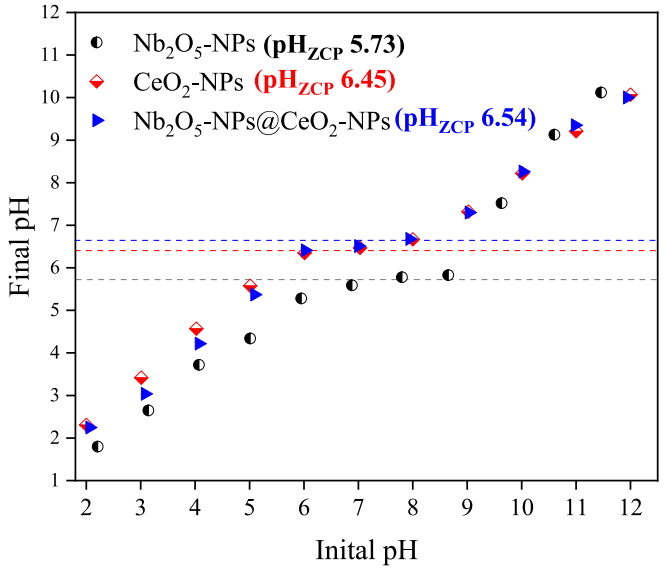

Fig. 2. Zero charge point of the samples (Nb_2O_5-NPs, CeO_2-NPs, Nb_2O_5-NPs@CeO_2-NPs).

addition, they can be prepared from green synthesis, using plant extracts as a reducing agent, such as pecan nutshell extract (*C. illinoiensis*), which is rich in polyphenols and flavonoids.[6].When combined with cerium oxide nanoparticles (CeO_2-NPs, E_g = 2.6 *eV*), their photocatalytic activity is increased, due to a reduction in the band gap of the nanocatalyst and an increase in its thermal and physicochemical stability, in addition to reducing costs associated with the nanocatalyst production process [7].

Despite the efficiency of this hybrid nanocatalyst, optimizing the removal of organic dyes requires time and costs associated with bench-scale experiments. In this view, recent advancements in decision tree-based machine learning (ML) algorithms (e.g., Decision Tree – DT, Random Forest – RF, and Extreme Gradient Boosting – XGBoost) have demonstrated significant potential in predicting catalytic activity in heterogeneous photocatalysis [8,9]. These models are capable of capturing complex dependencies in experimental data, enabling accurate predictions of nanocatalyst properties and performance under varying operational conditions, including in the prediction of the degradation efficiency of organic pollutants in wastewater treatment [10,11].

In this context, the present work aims to synthesize and characterize a niobium-based nanocatalyst doped with cerium oxide nanoparticles (Nb_2O_5-NPs@CeO_2-NPs) from *C. illinoinensis* extract for the removal of EBT from wastewater under visible radiation. Thus, the novelty of this study is that it relates nanobiotechnology to the Sustainable Development Goals (SDGs), focusing on ensuring the availability and sustainable management of water and sanitation for all, by developing a sustainable alternative nanomaterial with potential application in wastewater treatment.

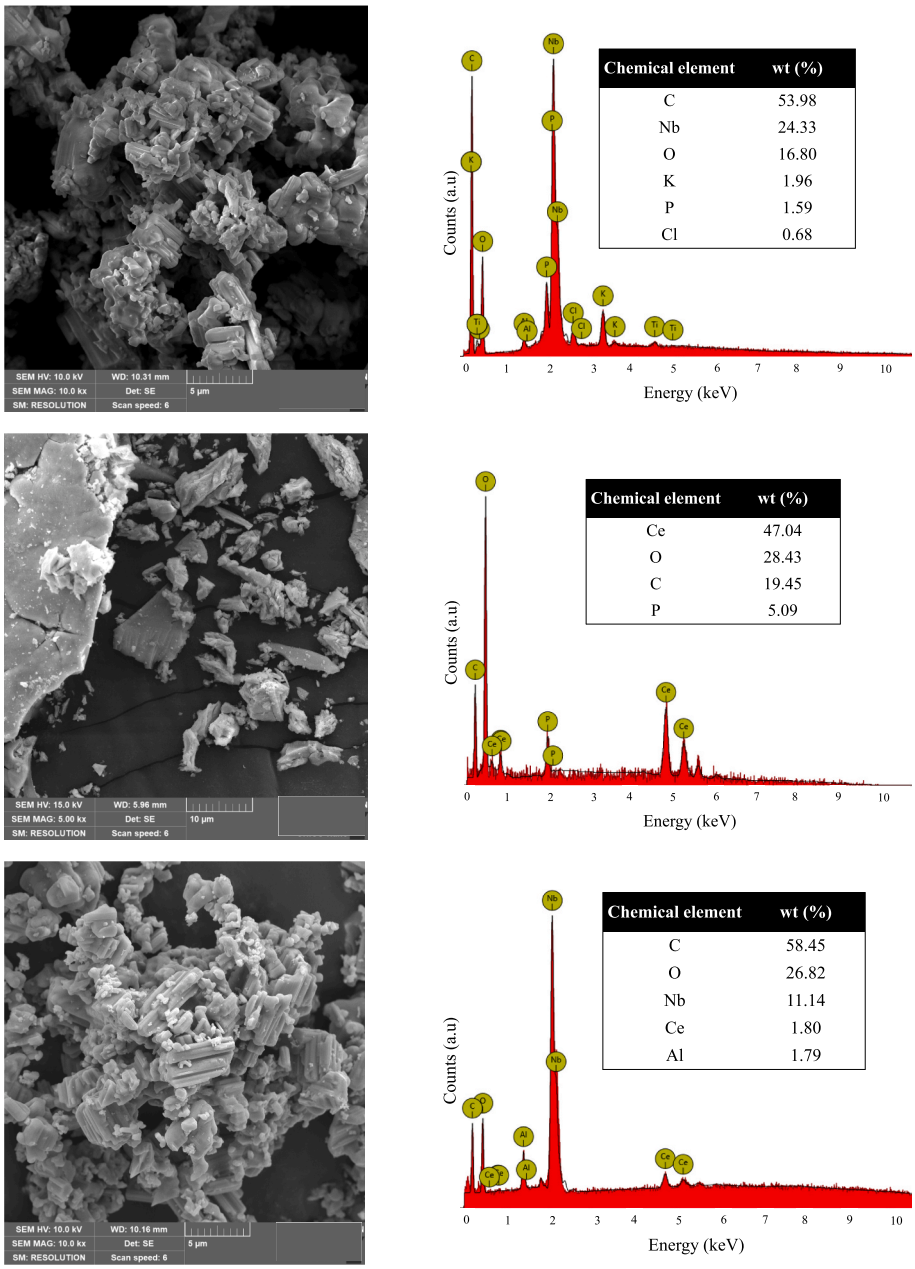

Fig. 3. (a) FEG micrographs with 10 kx magnification of the Nb_2O_5-NPs, (b) EDS results of Nb_2O_5-NPs, (c) FEG micrographs with 5 kx magnification of the CeO_2-NPs, (d) EDS results of CeO_2-NPs, (e) FEG micrographs with 10 kx magnification of the Nb_2O_5-NPs@CeO_2-NPs and (f) EDS results of Nb_2O_5-NPs@CeO_2-NPs.

Table 2
Textural and surface properties of Nb_2O_5-NPs, CeO_2-NPs, Nb_2O_5-NPs@CeO_2-NPs.

Sample	S_{BET} (m^2 g^{-1})	V_p (cm^3 g^{-1})	D_p (nm)	ZP (mV)
CeO_2-NPs	19 ± 0.40	0.04 ± 0.002	8.5 ± 0.50	−5.6 ± 0.3
N_2bO_5.NPs	171 ± 0.40	0.3 ± 0.010	9.7 ± 0.61	−28.2 ± 0.9
N_2bO_5.NPs@CeO_2-NPs	102 ± 0.33	0.2 ± 0.004	9.2 ± 0.65	−22.7 ± 1.0

2. Material and Methods

2.1. Preparation of the C. illinoiensis extract

To prepare the *C. illinoiensis* extract (donated from the pecan nut processing industry in southern Brazil), it was obtained through the infusion method [12], where 10 *g* of pecan nutshells were mixed with 500 *mL* of distilled water under magnetic stirring (120 *rpm* / 60 min / 80 ± 2°*C*). After, the solution was vacuum-filtered (Qualy, 90 *mm* circle) and stored in an amber flask at 25 ± 2°*C*.

2.2. Biosynthesis of the CeO_2-NPs and Nb_2O_5-NPs

The biosynthesis method [13,14] was used to develop the CeO_2-NPs and Nb_2O_5-NPs. For the CeO_2-NPs, 50 *mL* of the *C. illinoiensis* extract (20 $g\ L^{-1}$) were mixed with 50 *mL* of cerium(IV) sulfate solution ($Ce(SO_4)_2$,

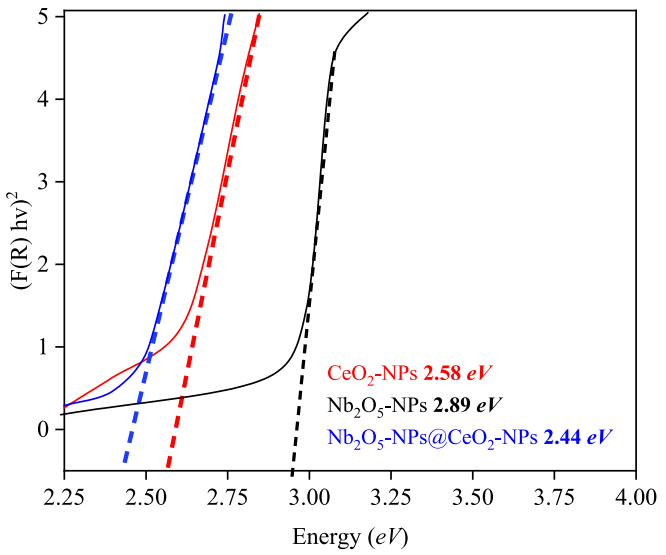

Fig. 4. Band gap energy evaluation for the nanocatalyst (Nb_2O_5-NPs@CeO_2-NPs) and its counterparts (Nb_2O_5-NPs, CeO_2-NPs).

Vetec, 0.1 *mol* L^{-1}) under magnetic stirring (300 *rpm*) for 60 min at 25 ± 2°*C*. Then, the sample was dried (75 ± 2°*C* for 720 min) and calcined (600°*C* / 180 min / 5°*C* min^{-1} in oxidant atmosphere). While for the Nb_2O_5-NPs, 50 *mL* of the *C. illinoiensis* extract were mixed with 50 *mL* of niobium(V) chloride solution ($NbCl_5$, Sigma-Aldrich, 0.1 *mol.*L^{-1}) and 5 *mL* of Ammonium Hydroxide solution (NH_4OH, Sigma-Aldrich, 30 %). Afterwards, the system was kept under magnetic stirring (200 *rpm*) for 60 min at 25 ± 2°*C*. Then, the sample was dried (90 ± 2°*C* for 720 min) and calcined (500°*C* / 120 min / 5°*C* min^{-1} in oxidant atmosphere).

2.3. Synthesis and characterization of Nb_2O_5@CeO_2-NPs

The supported heterogeneous nanocatalyst (Nb_2O_5-NPs@CeO_2-NPs) was synthesized by the impregnation method [15], where the CeO_2-NPs were used as the photoactive phase and Nb_2O_5-NPs the catalytic support. 0.2 *g* of the CeO_2-NPs and 1.0 *g* of the Nb_2O_5-NPs were added to 100 *mL* of distilled water under magnetic stirring (110 *rpm*, 25 ± 2°*C* for 90 min). After, the mixture was calcinated at 400°*C* for 4 h (30°*C* min^{-1}).

The heterogeneous nanocatalyst and its counterparts were characterized by XRD, DRS, N_2 porosimetry, ZP and pH_{ZCP}. The average crystallite size (d_c) was evaluated by Debye-Scherrer method, conforming Eq. (1).

$$dc = \frac{K^{*}\lambda}{\beta^{*}\cos(2\theta)} \quad (1)$$

More information on methodological aspects of the characterization techniques is available in the Supplementary Information (SI).

2.4. Photocatalytic assay

The photocatalysis tests were performed in a batch system with EBT dye (20 mg L^{-1}) as a target pollutant, and Nb_2O_5@CeO_2-NPs (1 *g* L^{-1}) as nanocatalyst. The photocatalytic process was divided into two stages, being: (a) adsorption: in the absence of irradiation for 60 min and (b) photocatalysis. under visible irradiation (Empalux® Bulb LED Lamp, 50 *W* Halogen Equivalent with 600*W* m^{-2}), aliquots (2 *mL*) were collected at predetermined times (0, 15, 30, 45, 60, 75, 90 and 120 min) and centrifuged (Spinlab, SL-16RAV) (4500 *rpm* for 5 min). The determination of EBT concentration was performed on a UV–Vis spectrophotometer (Shimadzu, UV–Vis Mini 1240) at 566 *nm* [16]. All of the experiments were performed in duplicate, and the results presented are the mean values (error value less than 5 %).

The experimental data were fitted according to the pseudo first-order (PFO) model proposed by Langmuir-Hinshelwood and the pseudo second-order (PSO) model, according to Eqs. (2–3) [17].

$$C_i = C_{i0}{}^{*}e^{-k^{*}t} \quad (2)$$

$$\frac{1}{C_i} = k_2{}^{*}t + \frac{1}{C_{io}} \quad (3)$$

Where: C_{i0} is the initial EBT dye concentration (*mg* L^{-1}), C_i is EBT dye concentration at time t (*mg* L^{-1}), *t* is the illumination time (min), *k* is the apparent rate of the PFO reaction (min^{-1}), k_2 is the apparent rate of the pseudo second-order reaction (*mL* g^{-1} min^{-1}).

2.5. Reuse of the nanocatalyst

The reuse of the nanocatalyst was evaluated in 5 cycles of heterogeneous photocatalysis up to 120 min under visible radiation, in the following operational conditions were used: [EBT] = 20 *mg* L^{-1}, [Nb_2O_5-NPs@CeO_2-NPs] = 1.0 *g* L^{-1}, pH 5, T = 25 ± 2°*C*, and V = 100 *mL*. In the cycle after each cycle, the solution was centrifuged (Spinlab, SL-16RAV) (4500 *rpm* for 5 min), and the solid (nanocatalyst) was carefully separated and reintroduced for the next cycle, with the percentage of degradation being measured after each cycle of heterogeneous photocatalysis.

2.6. Scavenger effect on heterogeneous photocatalysis

To investigate the participation of reactive oxygen species (ROS) and electron-hole pairs in dye photocatalytic degradation, a study of the use of scavengers in heterogeneous photocatalysis was carried out. Thus, 7.6 *mL* of isopropyl alcohol (•OH scavenger), 29.4 *mg* of potassium dichromate (e^- scavenger), 17.6 *mg* of ascorbic acid ($O_2^{\bullet}$ scavenger), and 29.2 *mg* of EDTA (h^+ scavenger) were employed to elucidate the photodegradation mechanism. The reduction or inhibition of degradation efficiency observed in the presence of these scavengers reveals the roles played by hydroxyl radicals (•OH), superoxide radicals ($O_2^{-\bullet}$), photogenerated electrons (e^-), and holes (h^+) in the reaction mechanism [18]. This methodology provides valuable insights into the photocatalytic pathways and clarifies the contribution of each reactive species to the overall degradation process.

2.7. Machine learning study

To propose a degradation reaction mechanism of EBT dye photodegradation, three ML algorithms were used: Decision Tree (DT), Random Forest (RF), and Extreme Gradient Boosting (XGBoost), whose detailed description is provided in Table 1. To enhance the reproducibility of the results, all machine learning models were initialized with the same random seed (random state = 42), ensuring consistent data shuffling and parameter initialization across runs. The ML algorithms were coded in Python 3.4, with numpy, pandas, sklearn and seaborn libraries used for compilation, data manipulation, and metrics evaluation.

The pH (6.15 – 13), reaction time (0 – 180 min), light source power (50 – 130 *W*), nanocatalyst concentration (0.1 – 1.50 *g* L^{-1}) and dye concentration (2 – 50 *mg* L^{-1}) were used as input variables, whereas the mass-charge ratio (*m/z*) was used as the response variable. The dataset was constructed using data collected (light source power, pH, reaction time, catalyst/dye concentration, retention time, and *m/z* signal) from scientific papers available in the literature (https://www.scopus.com), using the descriptors "Eriochrome Black T" AND "GC–MS" AND "degradation" AND "visible light", according to the Boolean Logic (no year limitation). The dataset (file Nunes_degradation_reaction_pathway.xlsx) is available on GitHub (https://github.com/Applied-Nanomat

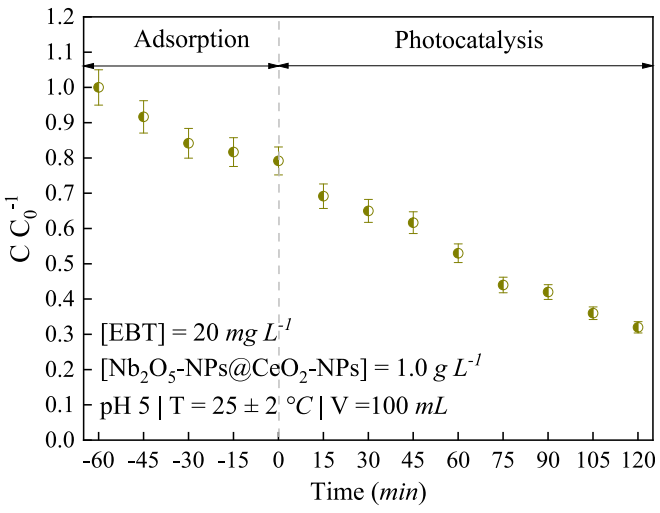

(a)

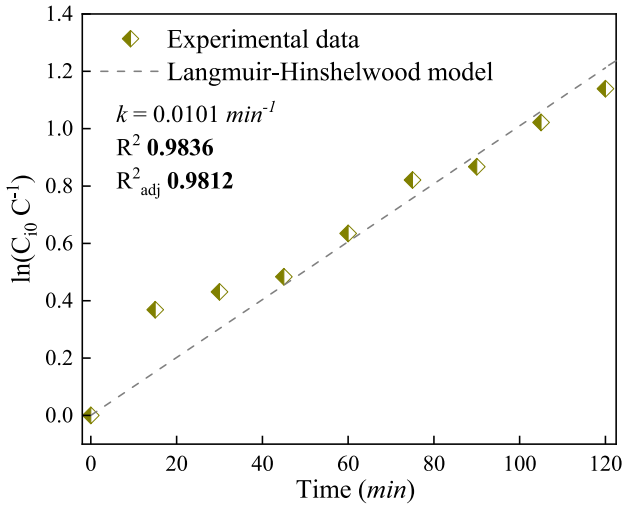

(b)

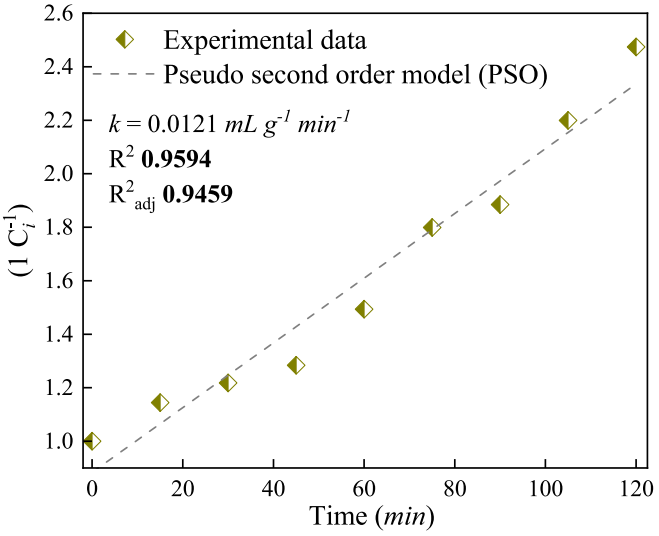

(c)

Fig. 5. (a) Degradation curve of the PFO model, (b) Langmuir-Hinshelwood curve fitting and (c) PSO model curve fitting for EBT dye experimental data ([Nb_2O_5-NPs@CeO_2-NPs] = 1.0 $g\ L^{-1}$, [EBT] = 20 $mg\ L^{-1}$, pH 7, 120 min | 600$W\ m^{-2}$).

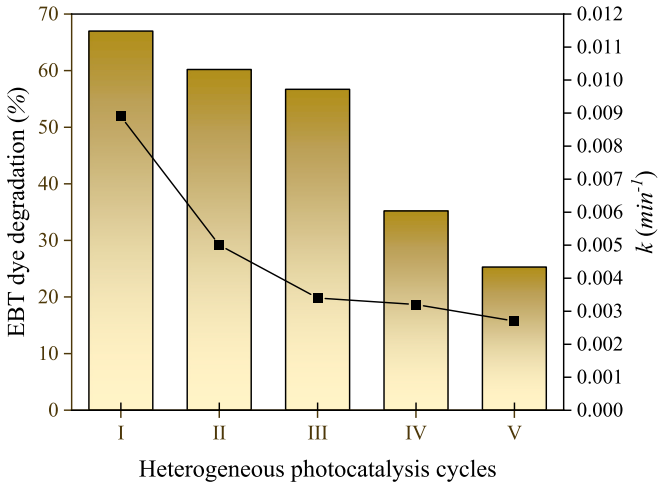

Fig. 6. Effect of the reuse of the Nb_2O_5-NPs@CeO_2-NPs nanocatalyst.

erials-Research-Group/Machine-and-Deep-Learning). The data was divided into training (80 %) and test (20 %) subsets, being preprocessed of data (descriptive analysis and data normalization – values from 0 to 1) was carried out using the Standard Scaler functions of the scikit-learn library, using the command MaxMinScaler for data resampling (values ranging from 0 to 1), in which the mean was converted to values near 0 and standard deviation near 1.

2.8. Phytotoxicity tests

To assess the potential harmful effects on seeds using Nb_2O_5-NPs@CeO_2-NPs and its counterparts (Nb_2O_5-NPs, and CeO_2-NPs), tests for phytotoxicity were carried out with 10 seeds of *Allium sativum* placed in a container with germination paper (Germitest®) in the range of 12.5–100 mg L^{-1} for 240 h under controlled temperature and humidity of 25 °C and 65 %, respectively In this context, the samples were checked for root growth measured with a digital caliper (Mitutoyo®) and compared to the negative control (NC) that had water and seeds. Additionally, the germination index (GI) was calculated using Eq. (8) [20].

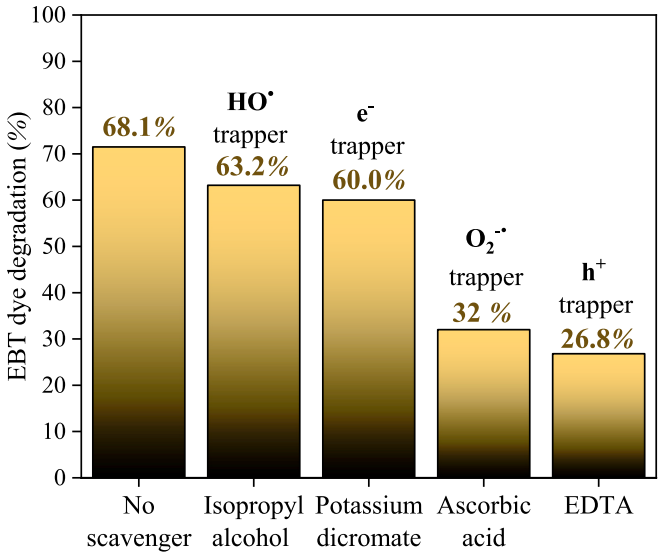

Fig. 7. Scavenger effect on the EBT photocatalytic degradation under visible radiation.

Table 3
Performance of the algorithms tested for MB photodegradation reaction pathway, in their optimal configuration.

Algorithm	$R^2_{training}$	R^2_{test}	$RMSE_{training}$	$RMSE_{test}$
DT	0.9688	0.7903	20.93	55.75
RF	0.9539	0.8364	25.46	49.24
XGBoost	0.8023	0.7785	53.97	53.65

$$GI(\%) = \frac{Seedgermination*Shootlenghtoftreatedwater}{Seedgermination*Shootlenghtofwater}*100 \quad (8)$$

3. Results and discussion

3.1. Characterization

Fig. 1 shows the diffractogram of the samples, where Nb_2O_5@CeO_2-NPs nanocomposite presented both crystalline phases of Nb_2O_5 and CeO_2-NPs, such as monoclinic niobium(V) oxide (Nb_2O_5 – JCPDS 33–1380, $d_c = 56.17 \pm 0.8$ nm) at 32.44° (001, d = 2.75 Å), 43.69° (100, d = 2.06 Å), 54.57° (101, d = 1.68 Å) and 56.75° (202, d = 1.62 Å) and tetragonal cerionite (CeO_2 – JCPDS 34–0394, $d_c = 50.77 \pm 0.7$ nm) at 28.34° (111, d = 3.15 Å), 33.03° (200, d = 2.71 Å) and 47.58° (220, d = 1.91 Å) confirming the impregnation of niobium combined with cerium nanoparticles. It is worth mentioning that the average crystallite size of both phases was around 50 nm, indicating nanometric-sized particles possibly due to the heat treatment used [21].

Fig. 2 shows the zero charge point of the nanocatalyst and its counterparts. Thus, the pH_{ZCP} increased from 5.73 to 6.54 when CeO_2-NPs were impregnated in Nb_2O_5-NPs and was similar to the pH_{ZCP} of CeO_2-NPs. The surface of the Nb_2O_5-NPs@CeO_2-NPs will be protonated at pH > 6,54 and deprotonated at pH > 6,54. Furthermore, the degradation of EBT under visible radiation is favored at the pH of the test (pH 5) due to the greater electrostatic interaction between the EBT molecule (anionic) and the surface of the nanocatalyst [22].

Studies involving the degradation of EBT under visible radiation are reported in the literature, where it was demonstrated that Nb_2O_5 doped with transition metals (such as Cu or Fe) has good photocatalytic activity for the degradation of dyes and other organic compounds at acidic pH, favoring the interaction with anionic pollutants due to the positive charge of the catalyst surface in acidic conditions [23].

Fig. 3 informs the micrographs and elementary composition of Nb_2O_5-NPs, CeO_2-NPs, Nb_2O_5-NPs@CeO_2-NPs where, Nb_2O_5-NPs display a more granular and agglomerated morphology, with particles forming dense clusters (Fig. 3a). Fig. 3(c) revealed that CeO_2-NPs exhibit irregular, plate-like structures with a heterogeneous surface. For the Nb_2O_5-NPs@CeO_2-NPs composite (Fig. 3e), the FEG-SEM micrographs demonstrated a morphology similar to Nb_2O_5-NPs, with pronounced aggregation and rough surfaces.

Additionally, EDS results shown in Fig. 3(f) confirmed the coexistence of Nb, Ce, and O, with Ce detected at 1.8 wt% in Nb_2O_5-NPs@CeO_2-NPs, verifying the successful impregnation of CeO_2-NPs onto the Nb_2O_5-NPs. The presence of Al and C suggests minor impurities or residuals from the synthesis process. Overall, the results demonstrate that CeO_2-NPs was effectively incorporated into the Nb_2O_5-NPs, as evidenced by both morphological and compositional changes.

Table 2 informs the textural properties and zeta potential of Nb_2O_5-NPs, CeO_2-NPs, Nb_2O_5-NPs@CeO_2-NPs.

According to Table 2, the specific surface area (S_{BET}) decreased from 171 $m^2\ g^{-1}$ to 102 $m^2\ g^{-1}$, suggesting that CeO_2-NPs partially blocked or occupied some of the active sites. Moreover, the pore volume (V_p) also showed a reduction (from 0.3 $cm^3\ g^{-1}$ to 0.2 $cm^3\ g^{-1}$), supporting this observation. Meanwhile, the average pore diameter (D_p) slightly decreased (from 9.7 to 9.2 nm), indicating slight structural modifications while retaining characteristics of the Nb_2O_5-NPs. Zeta potential (ZP) for Nb_2O_5-NPs (−28.2 mV) and Nb_2O_5-NPs@CeO_2-NPs (–22.7 mV) were higher (in modulus) than CeO_2-NPs (−5.6 mV), suggesting that both nanomaterials are stable in aqueous solutions [24].

Regarding the doping agent (CeO_2-NPs), the S_{BET}, V_P and D_p and ZP increased, which is positive for photocatalytic applications. This is because the increased surface area, pore volume, and pore size provide more active sites and enhanced mass transfer, while the higher zeta potential reduces the probability of nanoparticle agglomeration [25].

Thus, these structural and surface modifications, combined with the reduced band gap, suggest an improved photocatalytic performance, enhancing reactive species generation and promoting efficient degradation of anionic dyes [26]. Fig. 4 shows the band gap energies of the samples.

As can be seen in Fig. 4, the band gap energy (E_g) of the Nb_2O_5-NPs reduced from 2.89 eV to 2.44 eV when CeO_2-NPs are impregnated on the niobium-based green nanocatalyst. This reduction indicates enhanced light absorption and hence photocatalytic efficiency. It occurs due to a change in the Fermi level, bringing the conduction band closer to the valence band and, consequently, promoting a reduction in the forbidden band energy [27]. As a consequence, lower energy is required to activate the nanocatalyst for the generation of electron-hole pairs, which

Table 4
Predictions performed for *m/z* ratio related to byproducts of EBT photodegradation.

[Catalyst] ($g\ L^{-1}$)	[EBT] ($mg\ L^{-1}$)	pH	Light power (W)	Time (min)	Observed *m/z*	Predicted *m/z*	Relative error (%)
0.6	10	6.8	100	0	461.38	461.38	0
				30	327.33	324.96	0.72
				45	304.00	302.27	0.56
				50	279.00	221.85	20.5
				90	167.00	167.33	0.19
				180	58.00	58.05	0.08

Dataset: data collected from scientific papers involving photocatalytic degradation of EBT dye, in which the main degradation products were identified by GC-MS

5 inputs: reaction time | dye concentration | catalyst concentration | pH | light source power

1 output: m/z ratio, associated with the molar mass of the compound identified

Data size: 160 data points (160 lines x 5 rows), normalized for values between 0 and 1

Machine Learning algorithm: Random Forest (RF) Regressor

RF hyperparameters: max. tree depth: 5 | learning rate: 1 % | number of estimators = 100

Metrics: $R^2_{training}$ = **0.9539**, $RMSE_{training}$ = 25.46 | $R^2_{testing}$ = **0.8364** | $RMSE_{testing}$ = 49.24

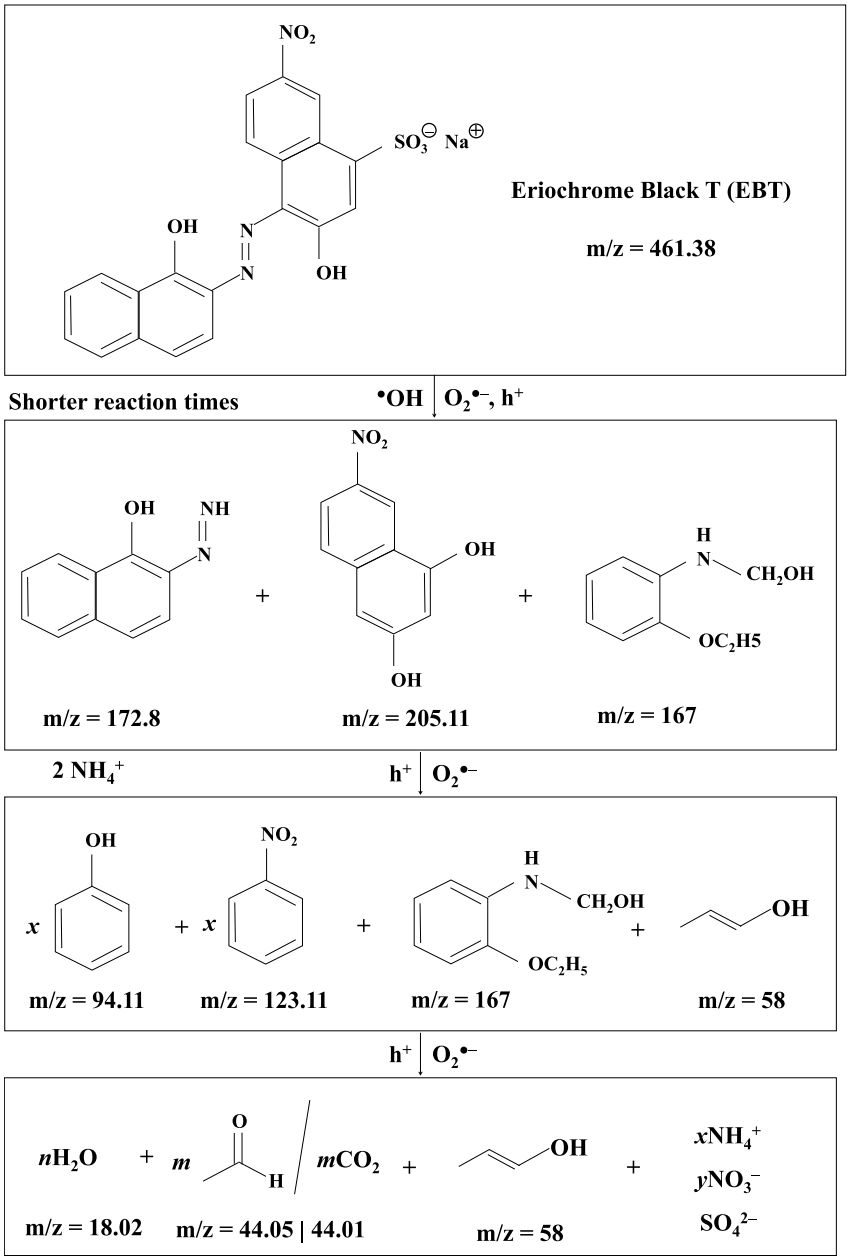

Fig. 8. General reaction pathway for EBT photocatalytic degradation proposed from RF algorithm.

enhances the production of reactive oxygen species (e.g., •OH and $O_2^{-\bullet}$) [28]. These species play a crucial role in breaking down the complex molecular structure of the EBT dye, leading to more efficient degradation and mineralization of the pollutant.

3.2. Photocatalytic degradation

Fig. 5(a), 5(b), and 5(c) show the degradation curve EBT dye photocatalytic degradation, and curve fitting of experimental data to the Langmuir-Hinshelwood kinetic and PSO model, respectively.

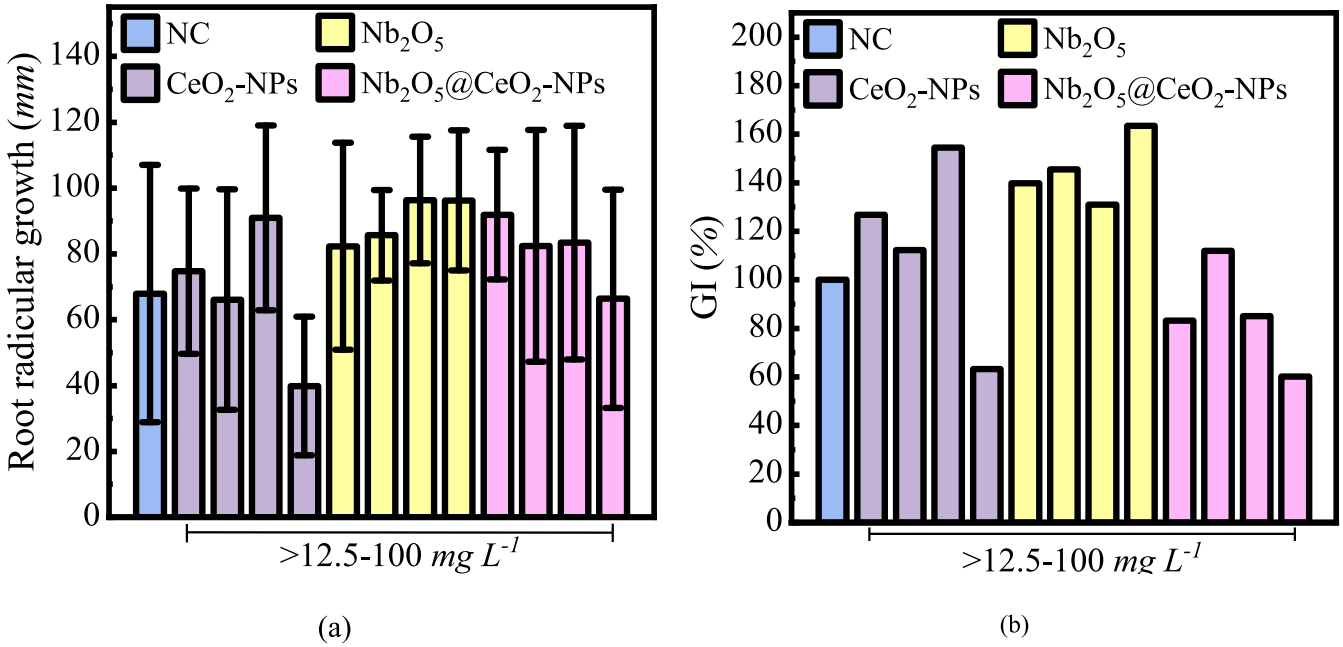

Fig. 9. (a) Radicular root growth of *Allium sativum*; and (b) GI of the CeO_2-NPs, Nb_2O_5, and Nb_2O_5@CeO_2-NPs. Statistical difference (one-way ANOVA) of $p < 0.033$*, $p < 0.002$** and $p < 0.001$***.

According to Fig. 5(a), about 70 % degradation of EBT dye was achieved at pH 5, [Nb_2O_5-NPs@CeO_2-NPs] = 1.0 $g\,L^{-1}$, [EBT] = 20 $mg\,L^{-1}$ after 120 min under visible radiation. Moreover, Fig. 5(b) showed that the experimental data of EBT photocatalytic degradation were well fitted by Langmuir-Hinshelwood kinetic model, reporting a kinetic rate constant $k = 0.0101\ min^{-1}$, with $R^2 = 0.9836$ and $R^2_{adj} = 0.9812$ [29]. This result suggests that the degradation process follows pseudo first-order (PFO) kinetics, with good efficiency in adsorption and degradation of the dye on the catalyst surface.

In parallel, Fig. 5(c) presents the curve fitting of experimental data to the PSO model, yielding a rate constant of $0.0121 mL\,g^{-1}\,min^{-1}$ with $R^2 = 0.9594$ and $R^2_{ajd} = 0.9459$. However, the curve fitting suggested that the EBT degradation reaction followed PFO kinetics since Langmuir-Hinshelwood model exhibited slightly better correlation with the experimental data than PSO model.

Studies in the literature reported similar results for the degradation percentage of the EBT dye, in which chemically synthesized CeO_2-NPs-based catalysts demonstrated smaller values for phenol (43–45 %) and methylene blue dye (48.5–56 % removal) after 120 and 180 min under visible light, especially when combined with metals as dopants to improve photon capture [30]. Furthermore, hybrid Nb_2O_5-NPs@CeO_2-NPs systems under visible light have shown synergy between the two phases, providing better charge separation and reducing electron-hole pair recombination [31].

The results of the present study suggest that the combination of Nb_2O_5-NPs with CeO_2-NPs not only extends the material's response to visible radiation but also optimizes the kinetics of EBT degradation. These findings reinforce the potential of these nanomaterials as efficient photocatalysts for the treatment of industrial effluents containing persistent dyes.

3.3. Reuse

Fig. 6 presents the reuse of the nanocatalyst for several cycles of heterogeneous photocatalysis. Thus, it was observed that the photocatalytic activity remained up to 3 cycles of heterogeneous photocatalysis, resulting in 59–68 % EBT dye degradation. After that, the photocatalytic activity of Nb_2O_5-NPs@CeO_2-NPs decreased considerably, probably due to photocatalyst surface deactivation caused by the occupation or blockage of active sites by reaction by-products and possible leaching of metals from the nanocatalyst (Nb^{5+} and Ce^{3+} ions), reducing the availability of reactive sites for further degradation reactions [32]. Thus, the result reported in the present work confirms the suitability of the synthesized green nanocatalyst for EBT degradation up to 3 cycles of photocatalytic degradation under visible radiation.

3.4. Effect of the scavengers

Fig. 7 shows the study of scavengers in the EBT dye degradation, where electron (e^-) and hydroxyl radicals ($HO^•$) generated from the activation of the photocatalyst showed little effect on EBT dye degradation, which is confirmed by the slight difference in the degradation percentage measured for EBT degradation using isopropyl alcohol (60 %) and potassium dichromate (63.2 %) compared to no scavenger (68.1 %). However, both EDTA and ascorbic acid lowered the EBT dye degradation percentage, suggesting that superoxide radicals ($O_2^{\bullet-}$) and hole (h^+) generated from the Nb_2O_5-NPs@CeO_2-NPs photoactivation show an important role in the dye photodegradation. This result is compatible with other reports in the literature, in which superoxide radicals are mainly responsible for the photocatalytic degradation of textile organic dyes [33]. In this view, the following section proposes a reaction pathway for EBT degradation under visible light.

3.5. Reaction pathway for EBT dye degradation

Table 3 shows the performance of the ML algorithms used in this work, where the RF algorithm shows the best performance among the ML algorithms since higher determination coefficients ($R^2_{training} = 0.9539$ and $R^2_{test} = 0.8364$) and lower RMSE ($RMSE_{training} = 25.46$ and $RMSE_{test} = 49.24$) values were reported.

Moreover, Table 4 shows the prediction performed by the RF algorithm, in which *m/z* ratio was predicted for specific catalytic and dye concentrations, pH, and time.

According to Table 4, the prediction performed shows low relative errors, confirming the suitability of the RF algorithm for the dye degradation reaction pathway. Thus, based on this, a degradation pathway for EBT dye was proposed, which is presented in Fig. 8.

According to Fig. 8, the EBT dye is decomposed into two relatively

high molecular weight compounds by breaking the C-N bond that connects the two aromatic rings. Thus, ((2-Methoxyphenyl)amino)methanol–dihydrogen(1/2) ($C_8H_{15}NO_2$, m/z = 167), 1-azotemino-2-hydroxynaphthalene ($C_{10}H_8N_2O$, m/z = 172.8), and 8-nitro-1,3-dihydroxynaphthalene ($C_{10}H_7NO_4$, m/z = 205.11) are formed.

In the first stage of the chemical reaction, the species $^{\bullet}OH$, $O_2^{\bullet-}$, and h + participate in the EBT photocatalytic degradation. Afterwards, the $O_2^{\bullet-}$ and h^+ showed major contribution on the EBT photodegradation, converting the 1-azotemino-2-hydroxynaphthalene and 8-nitro-1,3-dihydroxynaphthalene into phenol (C_6H_6O, m/z = 94.11), nitrobenzene ($C_6H_5NO_2$, m/z = 123.11), ((2-Methoxyphenyl)amino)methanol–dihydrogen(1/2) ($C_8H_{15}NO_2$, m/z = 167), and 1-propenol (C_3H_6O, m/z = 58), respectively. At higher reaction times, these products are degraded into lower molecular mass compounds, such as water (H_2O, m/z = 18.02), carbon dioxide (CO_2, m/z = 44.01), and/or acetaldehyde (C_2H_4O, m/z = 44.05), and 1-propenol (C_3H_6O, m/z = 58), respectively. This reaction pathway is consistent with experimental observations, since ~ 68 % dye degradation was reported. However, part of the sulfur and nitrogen atoms present in the chemical structure of the EBT dye are converted to ammonium (NH_4^+), sulfate (SO_4^{2-}), and nitrate (NO_3^-) ions. These degradation products and decreasing tendency in the molecular mass over time were observed in some EBT photocatalytic degradation studies reported in the literature [34,35].

3.6. Phytotoxicity of CeO_2-NPs, Nb_2O_5, Nb_2O_5@CeO_2-NPs

Seed germination and development capacity are crucial factors in *Allium sativum* seeds. Thus, the results of the phytotoxicity study are illustrated in Fig. 9(a), where it was observed that in the CeO_2-NPs concentration of 100 $mg\ L^{-1}$ resulted in reduced plant growth. Additionally, the germination index depicted in Fig. 9(b) indicated a moderate level of phytotoxicity for both CeO_2-NPs and Nb_2O_5@CeO_2-NPs at the same concentration of 100 $mg\ L^{-1}$ [36]. These results are linked to specific properties and characteristics of the seed types, including particle size, surface area, surface charge, and particle agglomeration, as well as maturation time, water absorption capacity, porosity, and the presence of essential micronutrients [37,38]. It is important to note that no studies were found addressing the phytotoxicity of niobium in these seeds. However, several researchers have observed the phytotoxicity of CeO_2-NPs at high concentrations, such as 1000 $mg\ L^{-1}$ [39,40]. Thus, at lower concentrations, Nb_2O_5@CeO_2-NPs can promote seed root growth as well as support plant development. Moreover, at low concentrations, Nb_2O_5@CeO_2-NPs can be used as a nanocatalyst without posing a threat to the environment.

4. Conclusion

In this work, a green niobium-based dopped with cerium oxide (Nb_2O_5-NPs@CeO_2-NPs) for EBT dye degradation under visible radiation was synthesized. The Nb_2O_5-NPs@CeO_2-NPs demonstrated good photocatalytic degradation of Eriochrome Black T dye under visible light, achieving 67 % removal efficiency, and a rate constant of 0.0101 min^{-1}, according to the pseudo-first-order kinetic model (R^2 = 0.9836 | R^2_{adj} = 0.9812), which represented the best fit of experimental data. Furthermore, the nanocatalyst maintained its photocatalytic activity for up to 3 cycles of heterogeneous photocatalysis under visible radiation, degrading 60–68 % of the dye molecule. Moreover, the study of the effect of scavengers reported that superoxide radicals ($O_2^{\bullet-}$) and holes (h^+) generated from Nb_2O_5-NPs@CeO_2-NPs photoactivation showed a key role in the dye degradation mechanism. Furthermore, RF ($R^2_{training}$ = 0.9539 | R^2_{test} = 0.8364 | $RMSE_{training}$ = 25.46 | $RMSE_{test}$ = 49.24) algorithm revealed that the main byproducts of the degradation reaction were water (H_2O, m/z = 18.02), carbon dioxide (CO_2, m/z = 44.01), and/or acetaldehyde (C_2H_4O, m/z = 44.05), and 1-propenol (C_3H_6O, m/z = 58). Therefore, this study demonstrates the potential of Nb_2O_5-NPs@CeO_2-NPs as an efficient and sustainable photocatalyst for environmental remediation, offering a promising alternative for the degradation of organic dyes in wastewater treatment. Moreover, decision tree-based algorithms can assist the photocatalytic degradation process for investigation of degradation reaction pathway.

CRediT authorship contribution statement

Adriano Losekann Mota Nunes: Writing – review & editing, Writing – original draft, Validation, Investigation, Formal analysis, Data curation, Conceptualization. **Leandro Rodrigues Oviedo:** Writing – review & editing, Writing – original draft, Validation, Methodology, Investigation, Formal analysis, Data curation. **Maurício Dalla Costa Rodrigues da Silva:** Writing – review & editing, Methodology, Formal analysis, Data curation. **Cristiane dos Santos:** Writing – review & editing, Formal analysis. **Giovani Pavoski:** Writing – review & editing, Formal analysis. **Denise Crocce Romano Espinosa:** Writing – review & editing, Formal analysis. **William Leonardo da Silva:** Conceptualization, Data curation, Formal analysis, Investigation, Validation, Writing – original draft, Writing – review & editing.

Declaration of competing interest

The authors declare that they have no known competing financial interests or personal relationships that could have appeared to influence the work reported in this paper.

Acknowledgments

The authors would like to thank the Franciscan University and University of Sao Paulo (LAREX - Laboratory of Recycling, Waste Treatment and Extraction) for the support and investment in the project. This study was financed by the Conselho Nacional de Desenvolvimento Científico e Tecnológico - Brazil (CNPq/MCTI/FNDCT n° 23/2022) - InovaNióbio (n° 408422/2022-0).

Appendix A. Supplementary data

Supplementary data to this article can be found online at https://doi.org/10.1016/j.inoche.2025.114779.

Data availability

Data will be made available on request.

References

[1] S. Dutta, S. Adhikary, S. Bhattacharya, D. Roy, S. Chatterjee, A. Chakraborty, D. Banerjee, A. Ganguly, S. Nanda, P. Rajak, Contamination of textile dyes in aquatic environment: Adverse impacts on aquatic ecosystem and human health, and its management using bioremediation, J. Environ. Manage. 353 (2024) 120103, https://doi.org/10.1016/j.jenvman.2024.120103.

[2] A. Silva, L.H.M.L.M. Santos, C. Antão, C. Delerue-Matos, S.A. Figueiredo, Ecotoxicological evaluation of chemical indicator substances present as micropollutants in laboratory wastewaters, Glob. NEST J. 19 (2017) 94–99, https://doi.org/10.30955/gnj.002051.

[3] N.A. Amancio, P.C. Colpa, C.M.S. Guardabaxo, C.B. Silva, L.G. Da Silva, Removal of eriochrome black T from aqueous solution using coffee husk as bioadsorbent, Rev. Agrogeoambiental. 16 (2024) e20241892–e20241898, https://doi.org/10.18406/2316-1817v16nunico20241892.

[4] H. Wang, X. Li, X. Zhao, C. Li, X. Song, P. Zhang, P. Huo, X. Li, A review on heterogeneous photocatalysis for environmental remediation: From semiconductors to modification strategies, Chinese, J. Catal. 43 (2022) 178–214, https://doi.org/10.1016/S1872-2067(21)63910-4.

[5] T. Tavakoli-Azar, A.R. Mahjoub, M.S. Sadjadi, M.B. Ghaznavi-Ghoushchi, Synergistic effect of band gap and surface area on the improvement of $NiTiO_3$ sunlight-driven photocatalysts via $NiTiO_3$@S nanocomposites, Inorg. Chem. Commun. 152 (2023) 110658, https://doi.org/10.1016/j.inoche.2023.110658.

[6] G. Yadav, M. Ahmaruzzaman, New generation advanced nanomaterials for photocatalytic abatement of phenolic compounds, Chemosphere 304 (2022) 135297, https://doi.org/10.1016/j.chemosphere.2022.135297.

[7] J. Mim, M.S. Sultana, P.K. Dhar, M.K. Hasan, S.K. Dutta, Green mediated synthesis of cerium oxide nanoparticles by using *Oroxylum indicum* for evaluation of catalytic

and biomedical activity, RSC Adv. 14 (2024) 25409–25424, https://doi.org/10.1039/d4ra04132a.
[8] B.R. Goldsmith, J. Esterhuizen, J.X. Liu, C.J. Bartel, C. Sutton, Machine learning for heterogeneous catalyst design and discovery, AIChE J. 64 (2018) 2311–2323, https://doi.org/10.1002/aic.16198.
[9] H. Mai, T.C. Le, D. Chen, D.A. Winkler, R.A. Caruso, Machine Learning for Electrocatalyst and Photocatalyst Design and Discovery, Chem. Rev. 122 (2022) 13478–13515, https://doi.org/10.1021/acs.chemrev.2c00061.
[10] K. Suzuki, T. Toyao, Z. Maeno, S. Takakusagi, K. Shimizu, I. Takigawa, Statistical Analysis and Discovery of Heterogeneous Catalysts Based on Machine Learning from Diverse Published Data, ChemCatChem 11 (2019) 4537–4547, https://doi.org/10.1002/cctc.201900971.
[11] J.Y.Y. Loh, A. Wang, A. Mohan, A.A. Tountas, A.M. Gouda, A. Tavasoli, G.A. Ozin, Leave No Photon Behind: Artificial Intelligence in Multiscale Physics of Photocatalyst and Photoreactor Design, Adv. Sci. 11 (2024) 2306604–2306618, https://doi.org/10.1002/advs.202306604.
[12] S. Caxambú, E. Biondo, E.M. kolchinski, R.L. padilha, A. Brandelli, V. Sant'anna, Evaluation of the antimicrobial activity of pecan nut [*Carya illinoinensis* (Wangenh) C. Koch] shell aqueous extract on minimally processed lettuce leaves, Food Sci. Technol. 36 (2016) 42–45, https://doi.org/10.1590/1678-457x.0043.
[13] D.M. Druzian, L.R. Oviedo, S.N. Loureiro, R.D. Wouters, B.S. Vizzotto, E.O. Pinto, N.J.S. De Vanconcellos, Y.P.M. Ruiz, A. Galembeck, G. Pavoski, D.C.R. Espinosa, C. dos Santos, W.L. da Silva, Cerium oxide nanoparticles: Biosynthesis, characterization, antimicrobial, ecotoxicity and photocatalytic activity, J. Photochem. Photobiol. A Chem. 442 (2023) 114773–114784, https://doi.org/10.1016/j.jphotochem.2023.114773.
[14] L.F.W. Brum, M.D.C.R. Da Silva, C. dos Santos, G. Pavoski, D.C.R. Espinosa, W.L. da Silva, Green synthesis of niobium (V) oxide nanoparticles using pecan nutshell (*Carya illinoinensis*) and evaluation of its antioxidant activity, Catal. Today 445 (2025) 115106- 445 (2025) 115109. DOI: 10.1016/j.cattod.2024.115106.
[15] W.L. Da Silva, M.A. Lansarin, J.H.Z. Dos Santos, F. Silveira, Photocatalytic degradation of rhodamine B, paracetamol and diclofenac sodium by supported titania-based catalysts from petrochemical residue: effect of doping with magnesium, Water Sci. Technol. 74 (2016) 2370–2383, https://doi.org/10.2166/WST.2016.362.
[16] Y.M. Hunge, A.A. Yadav, S.-W. Kang, Photocatalytic Degradation of Eriochrome Black-T Using $BaWO_4/MoS_2$ Composite, Catalysts 12 (2022) 1290–1300, https://doi.org/10.3390/catal12101290.
[17] N.G. Asenjo, R. Santamaría, C. Blanco, M. Granda, P. Álvarez, R. Menéndez, Correct use of the Langmuir–Hinshelwood equation for proving the absence of a synergy effect in the photocatalytic degradation of phenol on a suspended mixture of titania and activated carbon, Carbon 55 (2013) 62–69, https://doi.org/10.1016/j.carbon.2012.12.010.
[18] X. Jia, F. Wang, X. Xu, C. Liu, L. Zhang, S. Jiao, G. Zhu, X. Wang, G. Yu, Highly Efficient Photocatalytic Degradation of Tetracycline by Modifying UiO-66 via Different Regulation Strategies, ACS Omega 8 (2023) 27375–27385, https://doi.org/10.1021/acsomega.3c02762.
[19] M.D.C.R. da Silva, D.M. Druzian, L.F.W. Brum, C. dos Santos, G. Pavoski, D.C. R. Espinosa, Y.P.M. Ruiz, A. Galembeck, W.L. da Silva, Green synthesis of ZrO_2/PdO-NPs for photodegradation of anionic dyes: Photocatalytic activity and machine learning modelling, J. Mol. Liq. 410 (2024) 125581–125599, https://doi.org/10.1016/j.molliq.2024.125581.
[20] M. Kumar, M.N.M. Ansari, I. Boukhris, M.S. Al-Buriahi, Z.A. Alrowaili, N. Alfryyan, P. Thomas, R. Vaish, Sonophotocatalytic Dye Degradation Using rGO-$BiVO_4$ Composites, Glob. Challenges. 6 (2022) 2100132–2100142, https://doi.org/10.1002/gch2.202100132.
[21] H.E. Ahmed, Y. Iqbal, M.H. Aziz, M. Atif, Z. Batool, A. Hanif, N. Yaqub, W. A. Farooq, S. Ahmad, A. Fatehmulla, H. Ahmad, Green Synthesis of CeO_2 Nanoparticles from the *Abelmoschus esculentus* Extract: Evaluation of Antioxidant, Anticancer, Antibacterial, and Wound-Healing Activities, Molecules 26 (2021) 4659–4671, https://doi.org/10.3390/molecules26154659.
[22] F. Azeez, E. Al-Hetlani, M. Arafa, Y. Abdelmonem, A.A. Nazeer, M.O. Amin, M. Madkour, The effect of surface charge on photocatalytic degradation of methylene blue dye using chargeable titania nanoparticles, Sci. Rep. 8 (2018) 7104–7112, https://doi.org/10.1038/s41598-018-25673-5.
[23] A.G.S. Prado, L.B. Bolzon, C.P. Pedroso, A.O. Moura, L.L. Costa, Nb_2O_5 as efficient and recyclable photocatalyst for indigo carmine degradation, Appl. Catal. B Environ. 82 (2008) 219–224, https://doi.org/10.1016/j.apcatb.2008.01.024.
[24] . Atiwurcha, J. Derksen, D. Vega-Maza, J. Vinogradov, Zeta Potential of Intact Carbonate Core Samples Saturated with Natural Aqueous Solutions with Varying Concentration of Negative Potential Determining Ions, (2022). DOI: 10.5194/egusphere-egu22-13060.
[25] J. Kim, H. Park, Enhanced mass transfer in nanofluid electrolytes for aqueous flow batteries: The mechanism of nanoparticles as catalysts for redox reactions, J. Energy Storage. 38 (2021) 102529, https://doi.org/10.1016/j.est.2021.102529.
[26] S. Maensiri, C. Masingboon, P. Laokul, W. Jareonboon, V. Promarak, P. L. Anderson, S. Seraphin, Egg White Synthesis and Photoluminescence of Platelike Clusters of CeO_2 Nanoparticles, Cryst. Growth Des. 7 (2007) 950–955, https://doi.org/10.1021/cg0608864.
[27] L. Spessato, L.H.S. Crespo, M.C. Silva, M.S. Gibin, F. Sato, M.E.G. Winkler, V. C. Almeida, Tuning photodegradation performance using carbon quantum dots and niobium pentoxide, J. Mater. Sci. Technol. 191 (2024) 157–167, https://doi.org/10.1016/j.jmst.2023.12.039.
[28] L. Zhang, H. Jia, C. Liu, M. Liu, Q. Meng, W. He, Enhanced generation of reactive oxygen species and photocatalytic activity by Pt-based metallic nanostructures: the composition matters, J. Environ. Sci. Heal. Part C. 37 (2019) 1–13, https://doi.org/10.1080/10590501.2018.1555317.
[29] N. Ramesh, C.W. Lai, M.R. Bin Johan, S.M. Mousavi, I.A. Badruddin, A. Kumar, G. Sharma, F. Gapsari, Progress in photocatalytic degradation of industrial organic dye by utilising the silver doped titanium dioxide nanocomposite, Heliyon. 10 (2024) e40998-e41018. DOI: 10.1016/j.heliyon.2024.e40998.
[30] S.N. Matussin, F. Khan, M.H. Harunsani, Y.-M. Kim, M.M. Khan, Visible-Light-Induced Photocatalytic and Photoantibacterial Activities of Co-Doped CeO_2, ACS Omega 8 (2023) 11868–11879, https://doi.org/10.1021/acsomega.2c07058.
[31] N.P. Ferraz, A.E. Nogueira, F.C.F. Marcos, V.A. Machado, R.R. Rocca, E.M. Assaf, Y. J.O. Asencios, CeO_2–Nb_2O_5 photocatalysts for degradation of organic pollutants in water, Rare Met. 39 (2020) 230–240, https://doi.org/10.1007/s12598-019-01282-7.
[32] V. Gadore, A.K. Singh, S.R. Mishra, M. Ahmaruzzaman, RSM approach for process optimization of the photodegradation of congo red by a novel $NiCo_2S_4$/chitosan photocatalyst, Sci. Rep. 14 (2024) 1118, https://doi.org/10.1038/s41598-024-51618-2.
[33] S. Ganesan, T. Kokulnathan, S. Sumathi, A. Palaniappan, Efficient photocatalytic degradation of textile dye pollutants using thermally exfoliated graphitic carbon nitride (TE–g–C_3N_4), Sci. Rep. 14 (2024) 2284–2296, https://doi.org/10.1038/s41598-024-52688-y.
[34] S. Jayaraman, A.R. Warrier, Dark catalytic degradation of industrial dye effluents using orthorhombic Tin monosulphide nanocatalyst, J. Mol. Liq. 301 (2020) 112360, https://doi.org/10.1016/j.molliq.2019.112360.
[35] M. Yousif, A.H. Ibrahim, S.S. Al-Rawi, A. Majeed, M.A. Iqbal, M. Kashif, Z. U. Abidin, M. Arbaz, S. Ali, S.A. Hussain, A. Shahzadi, M.T. Haider, Visible light assisted photooxidative facile degradation of azo dyes in water using a green method, RSC Adv. 14 (2024) 16138–16149, https://doi.org/10.1039/d4ra01202j.
[36] H. Zeghioud, N. Khellaf, A. Amrane, H. Djelal, M. Bouhelassa, A.A. Assadi, S. Rtimi, Combining photocatalytic process and biological treatment for Reactive Green 12 degradation: optimization, mineralization, and phytotoxicity with seed germination, Environ. Sci. Pollut. Res. 28 (2021) 12490–12499, https://doi.org/10.1007/s11356-020-11282-1.
[37] M. Liu, S. Feng, Y. Ma, C. Xie, X. He, Y. Ding, J. Zhang, W. Luo, L. Zheng, D. Chen, F. Yang, Z. Chai, Y. Zhao, Z. Zhang, Influence of Surface Charge on the Phytotoxicity, Transformation, and Translocation of CeO_2 Nanoparticles in Cucumber Plants, ACS Appl. Mater. Interfaces. 11 (2019) 16905–16913, https://doi.org/10.1021/acsami.9b01627.
[38] Z. Li, W. Yan, Y. Li, Y. Xiao, Y. Shi, X. Zhang, J. Lei, K. Min, Y. Pan, X. Chen, Q. Liu, G. Jiang, Particle Size Determines the Phytotoxicity of ZnO Nanoparticles in Rice (*Oryza sativa* L.) Revealed by Spatial Imaging Techniques, Environ. Sci. Technol. 57 (2023) 13356–13365, https://doi.org/10.1021/acs.est.3c03821.
[39] S. Ravichandran, P. Thangaraj, P. Sengodan, J. Radhakrishnan, Biomimetic facile synthesis of cerium oxide nanoparticles for enhanced degradation of textile wastewater and phytotoxicity evaluation, Inorg. Chem. Commun. 146 (2022) 110037, https://doi.org/10.1016/j.inoche.2022.110037.
[40] R. Siranjeevi, V. Vasumathi, S. Suganya, A. Saravanan, R. Usha, M. Azhagurajan, R. Jeyalakshmi, Evaluation of biosynthesized GO@CeO_2 nanocomposites as a catalyst for UV-assisted degradation of organic dyes and phytotoxicity studies, Surf. Interfaces 44 (2024) 103748, https://doi.org/10.1016/j.surfin.2023.103748.

Adriano Losekann Mota Nunes Academic in the civil engineering course at Franciscan University

Leandro Rodrigues Oviedo Chemical Engineer from Franciscan University (2013-2018). Master in Nanosciences from Franciscan University (UFN). Worked as a Chemistry Teacher for the Alternative Popular Pre-University Extension Program (PUPA). Worked as a paid monitor in the disciplines of calculus I and II for engineering (2014-2015). Has the following extension courses: Unifra Languages - module I (2014); Basic Arduino (2015); Modeling and Simulation in Engineering Processes - Franciscan University (2016). Hygiene, health and beauty products (2017); Readings in English (2017). English Language Course at Topway English School-Santa Maria (2018). Supervised Curricular Internship in Quality, Safety, Environment and Health carried out at Thor Máquinas e Montagens LTDA (2018). Currently pursuing a PhD in the Postgraduate Program in Nanosciences. Research Line: reuse of waste for the synthesis of nanostructured materials.

Maurício Dalla Costa Rodrigues da Silva Maurício Dalla Costa Rodrigues da Silva is Occupational Safety Engineer at the Federal University of Health Sciences of Porto Alegre (UFCSPA). He graduated in Chemical Engineering from the Federal University of Santa Maria (UFSM), where he also completed his master's and PhD in Chemical Engineering. He conducted a postdoctoral fellowship in Nanoscience at Franciscan University (UFN). His expertise lies in process development, machine learning, and by-product valorization.

Cristiane dos Santos Dos Santos holds a degree in Bioprocess Engineering and Biotechnology from the State University of Rio Grande do Sul (2010). Postgraduate MBA in Expertise, Auditing and Environmental Management (2012), Master in Materials Science - PGCIMAT-UFRGS (2014) and PhD in Materials Science - PGCIMAT - UFRGS (2021). She has experience in Product Research and Development, Sustainable Processes and Sol-Gel Processes to obtain hybrid and composite nanomaterials. CNPq Industrial Technological Development Scholarship - DTI-A - Franciscan University - UFN-RS (2023-2024).

Giovani Pavoski Atiwurcha, J. Derksen, D. Vega-Maza, J. Vinogradov, Zeta Potential of Intact Carbonate Core Samples Saturated with Natural Aqueous Solutions with Varying Concentration of Negative Potential Determining Ions, (2022). DOI: 10.5194/egusphere-egu22-13060Postdoctoral fellow in the Department of Materials Engineering at the University of British Columbia, Vancouver (UBC, 2023-2024). Postgraduate professor in the Department of Chemical Engineering of the Polytechnic School of the University of São Paulo in the subjects: Analytical Techniques in Environmental Chemical Engineering I and Analytical Techniques in Environmental Chemical Engineering II (2022-present). Bachelor's degree in Industrial Chemistry from the Pontifical Catholic University of Rio Grande do Sul (PUCRS-2012), master's degree (2014) and doctorate (2019) in Materials Science from the Federal University of Rio Grande do Sul (UFRGS-2019). Sandwich doctorate at the Autonomous University of Barcelona (UAB-Spain) in the Sandwich Doctorate Program Abroad (PDSE - CAPES). Experience with synthesis, characterization and processing of nanoparticles and polymeric nanocomposites. Dissertation and Thesis in the area of polymeric nanocomposites (polyethylene), with emphasis on the acquisition of electrical conductivity (graphene nanosheets) and antibacterial properties (silver nanoparticles covalently bonded or encapsulated in silica). Experience with synthesis, processing and characterization of polymers. Microbiology evaluating the antibacterial properties of nanocomposites. Research in the area of environmental chemistry with recycling and analysis of metals. Recycling of industrial catalysts through pyro/hydrometallurgical processes. Synthesis of metallic nanoparticles using secondary sources (catalyst waste, electronics, polymer composites) as raw material, aiming at a circular economy. Synthesis of magnetic nanoparticles for selective separation of critical metals. Currently a post-doctoral researcher participating in the FAPESP project, application of functionalized magnetic nanoparticles for the selective separation of lanthanum from solution resulting from the leaching of spent catalysts, at the Laboratory of Recycling, Waste Treatment and Extraction (LAREX), Department of Chemical Engineering of the Polytechnic School (POLI-USP) and University of British Columbia (UBC).

Denise Crocce Romano Espinosa Espinosa holds a degree in Metallurgical Engineering from the University of São Paulo (1995), and a master's and PhD in Metallurgical Engineering from the University of São Paulo, in 1998 and 2002, respectively. She did an 8-month research internship at the Massachusetts Institute of Technology (USA) in 2001 and was a visiting professor at the University of British Columbia (Canada) for a period of 12 months (2015-2016). From 2009 to 2014, she was an Associate Professor in the Department of Metallurgical and Materials Engineering of the Polytechnic School of USP. She was coordinator of the Postgraduate Program in Metallurgical Engineering of the Polytechnic School of USP (2012-2014), and alternate coordinator of the Research Committee of the Department of Metallurgical and Materials Engineering of EPUSP (2009-2012). She is currently an Associate Professor in the Department of Chemical Engineering at EPUSP, a full member of the Coordinating Committee of the Graduate Program in Chemical Engineering at EPUSP (2014-present) and Vice-Head of the Department of Chemical Engineering at EPUSP (2018-2022). She works as a Technical Advisor to the Office of the Superintendence of Environmental Management at USP (2018-2023) and is a representative of USP to the State Environmental Council (2020-2023). Her main areas of expertise are: recycling, waste treatment, hydrometallurgy, extractive metallurgy, and recycling of electro-electronic equipment.

William Leonardo da Silva Da Silva holds a degree in Chemical Engineering from the Federal University of Santa Maria (2010), a master's degree (2012) and a PhD (2016) in Chemical Engineering from the Federal University of Rio Grande do Sul. He developed research as a sandwich doctoral student abroad (PDSE/CAPES - 2015) at Ulster University with NIBEC (Nanotechnology and Integrated Bioengineering Centre). He is currently an adjunct professor II at the Franciscan University and a permanent professor of the Postgraduate Program in Nanosciences, coordinating the research group in applied nanomaterials (GPNAp). He has experience in the area of Green Nanotechnology, with emphasis on green synthesis of metallic nanoparticles, chemical kinetics and catalysis, working mainly on the following topics: removal of organic pollutants in wastewater by Advanced Oxidative Processes (heterogeneous photocatalysis) and by adsorption process, metallic nanoparticles and nanocatalysts.